ELSEVIER

Geomorphology 21 (1998) 217–232

GEOMORPHOLOGY

Scale-dependent analysis of satellite imagery for characterization of glacier surfaces in the Karakoram Himalaya

Michael P. Bishop [a,*], John F. Shroder Jr. [a], Betty L. Hickman [b], Luke Copland [c]

[a] *Department of Geography and Geology, University of Nebraska at Omaha, Omaha, NE 68182-0500, USA*
[b] *Department of Computer Science, University of Nebraska at Omaha, Omaha, NE 68182-0500, USA*
[c] *Department of Earth and Atmospheric Sciences, University of Alberta, Edmonton, Alta. T6G 2E3, Canada*

Received 23 January 1997; revised 12 May 1997; accepted 23 May 1997

Abstract

Information regarding process–structure relationships and change in the Karakoram Himalaya is of great importance in studying glacier hydrology, mass balance, and dynamic environmental change. Such information is not readily available. Detailed spatio-temporal assessment requires field investigation coupled with quantitative remote sensing studies. We conducted an investigation of the large Batura Glacier in Pakistan to determine if spectral variability can be quantified and used to characterize glacier surfaces. Specifically, SPOT Panchromatic satellite data were evaluated for differentiating features of glacier structure resulting from ice movement, ablation, and supraglacial fluvial action. Image semivariogram analysis was conducted for assessing spectral variability patterns and fractal analysis was used to examine scale-dependent variation in the data. Results indicate that spectral variability from fields of ice seracs can exhibit fractal characteristics, although most surface features on the glacier exhibit a change in the fractal dimension over different ranges in scale. The fractal dimension was found to be useful for differentiating between glacier surfaces such as white ice and debris-covered ice. Characteristics of the debris-load and the scale-dependent nature of calculating the fractal dimension ultimately determined the potential of class separability. © 1998 Elsevier Science B.V.

Keywords: remote sensing; alpine glaciers; semivariogram analysis; fractal dimension

1. Introduction

Glaciers affect climate change (Budd and Smith, 1981) and landform development (Harbor, 1992). In addition, they often have a direct impact on human settlement. This is frequently the case in the Himalaya, because glacial meltwater is required for irrigation and hydro-electric projects. Rapid glacier advances and retreats can lead to major slope failures. Similarly, advances can block rivers and cause catastrophic break-out floods that transport large quantities of sediment. Information regarding relationships of the glacier process–structure is also critical to ongoing studies of denudation in the Himalayas (Zeitler, 1985; Zeitler and Chamberlin, 1991), and to assessing the efficiency of glacier sediment transfer. We lack a detailed understanding of glaciers over large parts of the Himalaya (Shroder

* Corresponding author.

PII S0169-555X(97)00061-5

et al., 1993), because of the inaccessibility of the terrain and government-imposed restrictions on aerial photography.

Remote sensing provides a potential solution to the monitoring of mountain glaciers by providing land cover and biophysical information at frequent intervals. Scale-dependent (spatio-temporal) information derived from satellite remote sensing, coupled with geomorphometric analysis and detailed field investigations, has the potential to greatly improve our ability to understand and monitor glacier process–structure relationships. Before widespread assessment and monitoring of glaciers becomes a reality, however, we must first determine how to extract spatial information from multispectral imagery, and how spectral and spatial information relate to geomorphic features.

Numerous investigators have evaluated the use of remotely sensed data for the study of alpine glaciers and glacial terrain (e.g., Krimmel and Meier, 1973; Ventura et al., 1987; Hall et al., 1990; Williams et al., 1991; Singhroy et al., 1992; Herzfeld et al., 1993; Bayr et al., 1994). Debris-covered glaciers, which are characteristic of those found in the Karakoram Himalaya, have not been thoroughly investigated by multispectral analysis (Bishop et al., 1995). Similarly, a paucity of quantitative remote sensing studies exist that were designed to examine and characterize the spatial statistical structure in satellite reflectance data as it relates to glacier phemonena. Studies of geomorphic processes are highly scale-dependent (Mark and Aronson, 1984) and we do not know the characteristic scale-dependencies associated with glaciers in the Himalaya. Consequently, we must relate electromagnetic variations recorded by satellite sensors to physical phenomena to study biophysical processes and monitor dynamic environmental change (Davis et al., 1991).

This paper examines the large Batura Glacier in Pakistan to determine if spectral variation in satellite data can characterize supraglacial characteristics. Specifically, the spatial statistical structure of SPOT Panchromatic data was examined and compared with field observations of different glacier surfaces. Our objectives were to: (1) determine if reflectance variation from glacier surfaces exhibits fractal response; and (2) evaluate the utility of scale-dependent variation to characterize the structural features of the glacier caused by factors such as supraglacial lithology, ice movement, ablation, the collapse of subglacial tunnels, and supraglacial fluvial action.

2. Study area

The present study was undertaken on the Batura Glacier, in the Karakoram Himalaya of northern Pakistan (Fig. 1). The Batura Glacier has received considerable attention over the last decade because of its effects on the strategic Karakoram Highway (KKH) between Pakistan and China. The glacier has blocked the Hunza Valley in the past, and destroyed roads and bridges. Chinese glaciologists (Batura Glacier Investigation Group, BGIG, 1979, 1980) predicted that the glacier would advance in the 1980s and retreat in the 1990s. Continued monitoring of the character and fluctuation of this glacier is important for assessing environmental change, for predicting future problems with the KKH, for assessing problems with irrigation meltwater, and for noting the effects of the glacier on village life in Batura Valley. Furthermore, the study of the Batura Glacier drainage basin is significant because it is the type area for designation and definition of the three main glaciations of the Pleistocene in this region, the Shanoz, Yunz, and Hunza (Zhang and Shi, 1980; Derbyshire et al., 1984; Shroder et al., 1993). Similarly, research on Batura Glacier is complementary to ongoing studies of glaciers on the nearby Nanga Parbat massif (Finsterwalder, 1937; Gardner, 1986; Gardner and Jones, 1993). Nanga Parbat is currently the focus of our research in modeling rapid rates of exhumation (Shroder, 1989; Shroder et al., 1993) associated with the rapid recent uplift of the mountain (Zeitler, 1985; Zeitler and Chamberlin, 1991).

3. Geomorphology

The 59 km length of Batura Glacier makes it one of the eight largest glaciers in the middle to low latitudes. The glacier flows from west to east below the north side of the peaks of Batura Mustagh (7795 m; Fig. 2), from a maximum altitude of $\sim$6200 m of the western ice flow down into the Hunza River

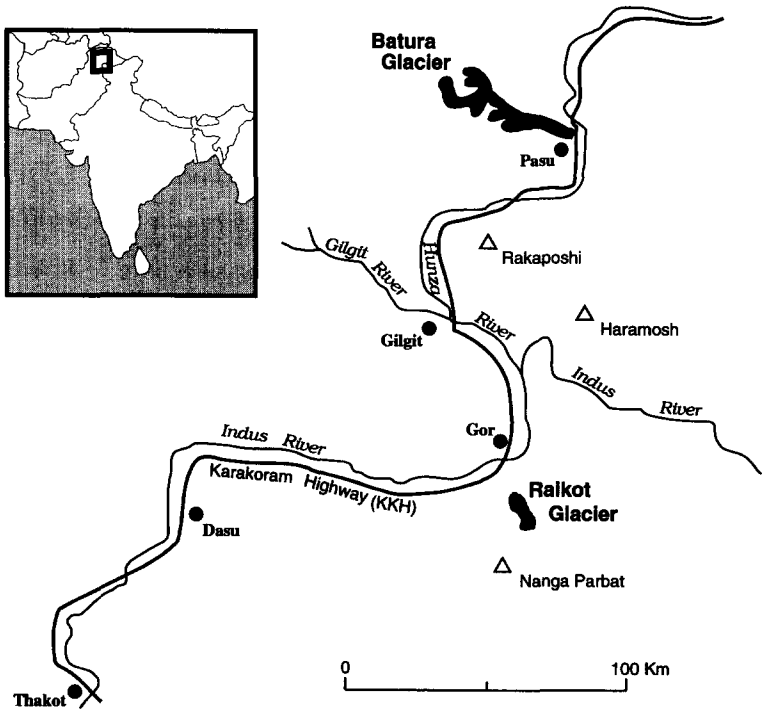

Fig. 1. Location of Batura Glacier in northern Pakistan.

valley at 2516 m. The drainage area totals ~690 km^2, with about 320 km^2 ice-covered, although the contiguous parts of Batura proper have an area of ~285 km^2. The glacier consists of five main ice flows (Fig. 2) and over 20 smaller tributary glaciers. The basin is masked with heavy ice cover on the higher north-facing slopes and much less extensive glaciers on the lower south-facing side. Many of the south-facing glaciers provide only debris and meltwater to the Batura. Ablation valley complexes of mixed mass wasting, fluvial, and lacustrine origin are concentrated between the south-facing slopes and the glacier edge. Such well watered valleys and the more gentle slopes associated with them are vital parts of western Himalayan agricultural systems. For more detailed information regarding climate and

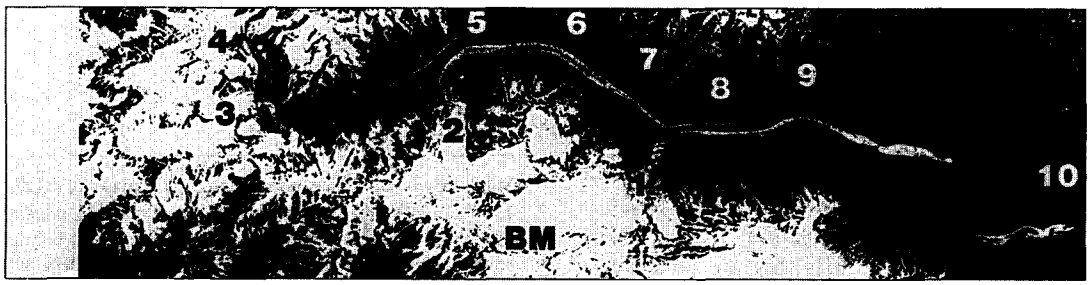

Fig. 2. SPOT Panchromatic image of Batura Glacier and surrounding area. Features and locations are depicted as follows: *BM* = Batura Mustagh (7795 m); *1* = first ice flow; *2* = second ice flow; *3* = western ice flow; *4* = northern ice flow; *5* = Yoksugoz ice flow; *6* = Shirin Maidan; *7* = Kukhil; *8* = Fatima; *9* = Yashpirt; *10* = Yunz.

glacier characteristics, such as supraglacial lithology and ice velocities, see Bishop et al. (1995).

3.1. Surface features of the glacier

We subdivide Batura Glacier into seven main topographic divisions (Table 1), the first six of which are ice features only: (A) northern ice flow, (B) western ice flow, (C) upper Batura Glacier to the second ice flow, (D) middle Batura Glacier from the second to the first ice flow, (E) lower Batura Glacier from the first ice flow to the end of the lowermost white-ice stream, and (F) the terminus zone. These six divisions reflect the diverse physical processes of the glacier ice that are reflected in surface characteristics and satellite image tone/texture combinations.

The dominant uppermost surface of the glacier is first characterized by the rather featureless cirques that pass downward through extending flow over ice falls where the glacier breaks up into seracs. These areas are commonly below the equilibrium line with the result that thin medial moraines first appear from beneath the firn and also pass downward into the broken-up crevasses. The western ice flow and its serac field pass downward as a thin white-ice stream to a position near where the tributary Yoksugaz ice flow joins from the north.

Seracs were not distinguished below the first and second ice flows, even though small areas of seracs do occur there. Instead, we followed the Chinese example (BGIG, 1979) and utilized only the large ogives that formed by compressive flow from the seracs below the first and second ice flows. The ogives pass down-ice into the reticulated ice hills of the first and second white-ice streams which are utilized in our analysis.

The remainder of our analysis concentrated upon the medial moraines in the upper part of the glacier near the first and second ice flows, and the lower zones of debris-covered ice closer to the terminus. The area in the southern half of the glacier down-ice from the termination of the first white-ice stream is characterized by the highest ablation (BGIG, 1979), with large curvilinear ice-cliffs that are concave in an up-glacier direction, and by rounded granodiorite clasts which relate to the extensive meltwater there (Bishop et al., 1995). To the immediate north of this

Table 1
Topographic divisions of Batura Glacier

A – Northern ice flow
(1) Tributary glaciers BN-I, BN-II

B – Western ice flow
(1) Tributary glacier BN-III

C – Upper Batura Glacier (to second ice flow)
(1) Tributary glacier BS-XI
(2) Tributary glacier BS-X
(4) Main upper Batura Glacier
(5) Laterally compressed medial moraines of C (4)

D – Middle Batura Glacier (second to first ice flow)
(1) Yoksugoz ice flow from north overwhelms and incorporates C (4)
(2) Lighter-colored Yoksugoz debris stream in northern part of Middle Glacier
(3) Part of C (4) debris-covered ice stream with up-ice curvilinear dark ice-cliffs
(4) Tributary glacier BS-VIII
(5) Ice avalanche and rock fall debris supply
(6) Tributary glacier BS-VII
(7) Tributary glacier BS-VI
(8) Tributary glacier BS-V

E – Lower Batura Glacier (first ice flow to end of lowermost white-ice stream)
(1) Tributary glacier BS-IV
(2) Tributary glacier BS-III to E1 south side debris-covered ice stream.
(3) Tributary glacier BS-II to E1 south side debris-covered ice stream
(4) First large white-ice flow, middle part
(5) First white-ice flow, lower part
(6) Middle medial moraine of lighter granodiorite
(7) Second white-ice stream continuation of D4 reticulated ice hills
(8) North side debris-covered ice stream

F – Batura Glacier terminus zone
(1) South dark-toned Passu slate debris-covered ice
(2) Lighter middle-rounded granodiorite with curvilinear dark ice-cliffs
(3) North darker-weathered granodiorite zone
(4) Stagnant terminus

G – Ablation valley complexes
(1) Northern system
(2) Southwestern system

Subdivisions are based upon geomorphic maps of BGIG (1979, 1980), field work, and interpretations of satellite imagery. Only the largest of these features are visible on Fig. 2 because of its small scale as published herein. Four nested orders of features have been differentiated but only the first two are presented here.

high ablation lobe occurs a low ablation lobe with thicker and more weathered granodiorite, and fewer and more irregular-shaped ice-cliffs.

3.2. Glacier debris-load

As is typical of so many of the largely avalanche-fed glaciers of the Himalaya, Batura Glacier carries large amounts of debris over most of its surface. Exceptions are the several white-ice streams that descend from the first and second ice falls from Batura Mustugh and the ice streams of the farthest north and west cirques. Field measurements show that, in general, debris thickness increases towards the terminus and the edges of the glacier. For example, the measured general debris thickness between Fatima and Yashpirt was ~ 1 m at the edge of the glacier, ~ 0.5–0.25 m above dark gray ice-cliffs midway out on the glacier, ~ 0.25 m above white ice-cliffs, out toward the middle of the glacier, and < 1 cm on the exposed white ice.

4. Remote sensing and glaciers

4.1. Background

The launch of the weather satellite TIROS-1 in 1960 provided images of Earth that demonstrated that snow-covered areas could be delineated from space (Fritz, 1962; Singer and Popham, 1963; Tarble, 1963). Since then, the launch of numerous Earth resource satellites (e.g., Landsat and SPOT) have provided moderate to high resolution multispectral imagery, necessary for monitoring mountain glaciers. Numerous glaciological studies used remotely sensed data to determine the velocities of ice surfaces (Krimmel and Meier, 1973; Scambos et al., 1992; Ferrigno et al., 1993; Lucchitta et al., 1993; Lefauconnier et al., 1994), the comparison of field- and satellite-measured reflectance of snow and ice bodies (Dozier, 1984; Brest and Goward, 1987; Hall et al., 1988, 1989, 1990; Koelemeijer et al., 1993), the mapping of ice and snow facies (Hall et al., 1987; Dozier and Marks, 1987; Dozier, 1989; Gratton et al., 1990; Williams et al., 1991; Parrot et al., 1993; Brugman et al., 1996), glacier mass balance studies (Ostrem, 1975; Kulkarni, 1992; Gratton et al., 1993; Bayr et al., 1994), supraglacial debris mapping (Nakawo et al., 1993; Bishop et al., 1995), and glacier inventory and detection of climate change (Vohra and Aggarwal, 1981; Espizua and Bengochea, 1990; Hastenrath, 1993).

An important component of many studies of the remote sensing of glaciers are field measurements close to the date of image acquisition. The collection of reference data usually involves detailed measurements regarding the physical characteristics of the glacier. It is problematic to associate the magnitude of reflectance with a particular snow or ice surface without prior knowledge of the physical characteristics of that surface. For example, Sigurdsson (1994) argued that Williams et al. (1991) may have misclassified several facies on an Icelandic glacier because of the absence of direct simultaneous ground observations. The boundary defined by Williams et al. (1991) as the transient snow-line because of a sharp contrast in spectral emissivity, may instead be related to the presence of a highly reflective crust of porous ice that is commonly superimposed on glacier ice over large areas on bright days in summer.

Recent studies have also focused on radiometric calibration of imagery to normalize the topographic effect (Dozier, 1989; Gratton et al., 1990; Parrot et al., 1993; Brugman et al., 1996). Digital elevation models (DEMs) have commonly been used to calculate the slope and azimuth of the reflecting surface (Gratton et al., 1990). Dozier (1989) points out that only poor digital elevation data are available for most mountain locations. As a partial solution to this problem, he estimated typical spectral signatures for a range of snow types, atmospheric profiles, and topographic illumination without the need for DEM data.

4.2. Work in the Himalaya

Depending upon the topographic complexity of the terrain, it is often possible to classify the surface of an observed glacier into one or more distinct zones. For example, Bayr et al. (1994) were able to subdivide the Pasterze Glacier, Austria, into three identifiable spectral classes that represented snow, bare ice, and morainal material or till. Similarly, Kulkarni (1992) used Landsat TM data to determine the position of the transient snow-line close to the

end of the ablation season on two Himalayan glaciers. This enabled the determination of the accumulation area ratio (AAR) of the glaciers, and, therefore, an estimate of the trends in mass balance as imagery from more 1 year was used. Certain limitations still remain in these applications, because of factors such as spatial resolution, cloud cover, variability in acquisition dates, and interannual climatic variability. Gratton et al. (1990) also stated that whereas multispectral classification works well for spectrally unique features, such as snow and alpine vegetation, traditional approaches will not yield high mapping accuracies for features that are spectrally heterogeneous and defined based on geomorphological criteria.

In this study, we use such geomorphological criteria and spatial analysis to assess supraglacial characteristics in the Karakoram Himalaya. Heavily debris-covered surfaces are characteristic of Himalayan glaciers, yet limited quantitative remote sensing research exists in the Himalaya. This information is important, however, for studies of glacier mass balance, estimates of regional rates of denudation, assessment of the role of glaciers in landscape and landform development, and understanding of ice flux/sediment discharge characteristics today and in the past. Nakawo et al. (1993) made one of the first remote sensing studies of a Himalayan debris-covered glacier in an attempt to improve estimates of the patterns of surface ablation. With the use of multispectral satellite data combined with detailed field measurements, they were able to classify the ablation area of Khumbu Glacier, Nepal, into snow, bare ice, thin debris and thick debris. The differentiation of thick from thin debris was not satisfactory, however, as closer examination showed that changes in rock lithology were the main features being detected, and that correlations of lithology with variations in debris thickness were coincidental. Bishop et al. (1995) improved on the characterization of supraglacial debris by using field measurements combined with high resolution SPOT Panchromatic and multispectral imagery to produce supraglacial debris-load estimates for the Batura Glacier, Pakistan. Visual analysis of panchromatic data identified unique tone/texture combinations that were associated with physical characteristics of the glacier surface (e.g., downwasting glacier surface, glacial outwash, etc.), whereas multispectral data enabled classifications depicting supraglacial lithology and shallow debris-load variability. Classification error was associated with the difficulty of characterizing deep debris depths.

5. Spatial feature extraction

With the advent of new satellite-based sensor systems, spectral analysis of glaciers has the potential to provide new insights and capabilities in detecting and mapping the characteristics of glaciers. Improvements in spatial, spectral, and radiometric resolution will increase spectral variability in images. This can cause difficulties in analysis, especially when traditional statistical and per-point classification algorithms are used. Spectral features generated from image transformations and per-point classification methods do not make use of all available image information because they disregard the spatial relationships that exist among pixels (Harris, 1980; Dutra and Mascarenhas, 1984). Therefore, extraction methods for spatial features must be able to represent local textural properties, contextual, and global information, so that spectral variability is incorporated into the analysis.

Researchers have worked in the area of spatial analysis for the last two decades (Sali and Wolfson, 1992). Early work focused on deriving spatial features to characterize local textural properties (e.g., Haralick et al., 1973; Weszka et al., 1976; Haralick, 1979; Conners and Harlow, 1980; Irons and Petersen, 1981) and evaluating the utility of these features for terrain and image classification (e.g., Shih and Schowengerdt, 1983; Dutra and Mascarenhas, 1984; Frank, 1984). Procedures for texture analysis are based primarily on structural or statistical methods (Haralick, 1979). The statistical approach is most widely used in remote sensing research and seeks to model local spectral variability as statistical features of the gray-level distribution. Sali and Wolfson (1992) summarize and describe the most widely used statistical features which include:

1. First-order statistics. Features such as the arithmetic mean, variance, and higher-order moments are calculated to exploit information about the local neighborhood of a single pixel.

2. Second-order statistics. Features that are based upon the use of a gray-level co-occurrence matrix. The features describe the relationships between neighboring pixels based upon a direction and distance.
3. Image convolution with different masks. Spatial filtering of images are useful for texture discrimination (Laws, 1980).
4. Fourier transform. Features that take into consideration the angular direction of the texture and the presence of directional objects in the texture. These features are based upon the Fourier power spectrum.
5. Multi-resolution and fractal-based features. Fractal theory may be used to describe the changes in texture with resolution. Because textures and surfaces may exhibit fractal behavior, the fractal dimension may be useful.

Investigators have determined that the use of spatial features can reduce misclassification and improve image analysis for some applications (Rosenfeld, 1980; Shih and Schowengerdt, 1983; Wang et al., 1983; Sali and Wolfson, 1992). Difficulties associated with using traditional statistical features include selection of the window size and boundary effects (McDermid and Franklin, 1995; Ryherd and Woodcock, 1996). In addition, these features provide a measure of the relative total variation, but do not provide information on spatial patterns and irregularities (Burrough, 1993). Consequently, it is difficult to use first-order, second-order, and convolution-based features to accurately characterize spectral and topographic variation that may be scale-dependent. Although investigators are continuing to develop and test new statistical procedures and features (e.g., Chorowicz et al., 1989; Wang and He, 1990; Andrle, 1994), issues involving scale dependence and the utility of geostatistics and fractals for characterizing and modeling spatial variation are important research problems (Davis et al., 1991).

Spatial patterns and/or textures can be described quantitatively by the semivariance function (De Jong and Burrough, 1995). For detailed discussions regarding semivariograms in remote sensing, see Curran (1988), and Woodcock et al. (1988a,b). Generation of the semivariogram is based upon the idea that the statistical variation in the data is a function of distance or sampling lag. Curran (1988) provides an introduction to the semivariogram in remote sensing and indicates that it provides information on spatial dependence. Several investigators have utilized the semivariogram and associated parameters for characterization and classification for ecological applications (e.g., Bowers et al., 1994; Cohen et al., 1990). In addition, the semivariogram can be used to estimate the fractal dimension, although few spatial feature extraction studies for glacier surfaces have been conducted.

In geomorphometry, investigators have evaluated the utility of fractal analysis and the use of the fractal dimension for characterizing the statistical response of geomorphic surfaces. Mark and Aronson (1984) investigated seventeen topographic surfaces and found that the majority of them exhibit scale-dependent fractal dimensions (i.e., the fractal model describes the statistical response of topography only within specific scale ranges). Since then other investigators have evaluated the fractal nature of topography and fractal modeling techniques (e.g., Goodchild, 1980; Goodchild and Mark, 1987; Mulla, 1988; Andrle and Abrahams, 1989; Yokoya et al., 1989; Polidori et al., 1991; Klinkenberg and Goodchild, 1992; Lam and Quattrochi, 1992; Bian and Walsh, 1993; Gregotski and Jensen, 1993; Jaggi et al., 1993).

In remote sensing a limited number of studies have been conducted to evaluate the utility of fractals for complex image analysis (De Jong and Burrough, 1995). Similarly, studies have focused on identifying scale dependence, determining whether landscape/land-cover units exhibit fractal response, and using the fractal dimension to improve classification accuracies (e.g., De Cola, 1989; Lam, 1990; Bian and Walsh, 1993; Olsen et al., 1993; Roach and Fung, 1994; De Jong and Burrough, 1995). Research indicates that topographic surfaces and spectral reflectance variation for land-cover units often exhibit fractal response over certain ranges of spatial scale. Such surfaces can be characterized by the fractal dimension, D, which corresponds to our intuitive perception of surface roughness. Consequently, research involving the characterization of geomorphic surfaces and the identification of scale-breaks using satellite reflectance data should provide new insight into operational scale and process–structure relationships (Davis et al., 1991). This is especially the case in the Himalaya, where access limitations and harsh

working conditions often make it difficult to obtain quantitative information for entire landscape and glacier surfaces. This paper investigates the use of the semivariogram and the fractal dimension to characterize glacier surfaces. For additional information on scale and fractal analysis, see Lam and Quattrochi (1992).

6. Methodology

6.1. Data acquisition

SPOT Panchromatic satellite data with a spatial resolution of 10 m were acquired on June 20, 1990. Radiometric calibration was not applied to the satellite imagery because differential illumination was not visible as a result of the low topographic gradient of the glacier surface. Furthermore, atmospheric influences were minimal because of the high altitude of the Batura Glacier.

Exploratory fieldwork was undertaken in the summers of 1991 and 1992, and detailed field work in May and June, 1993, when we conducted our remote sensing field survey. While traversing the length of Batura Glacier, we recorded global positioning satellite (GPS) measurements for sample sites and static features to establish geodetic control. Observations at sample locations consisted of recording the depth of glacial debris, lithology, topographic profile information, and characteristics of the surface structure. In addition, ground photography and high altitude steep angle oblique photos (i.e., ~ 4500 m) were obtained. The velocity of the Batura Glacier and ablation information were obtained from detailed field investigations conducted by the BGIG (1979, 1980). This information served as reference data for subsequent digital analysis of satellite imagery.

6.2. Semivariogram analysis

Visual interpretation of the satellite imagery revealed unique tone/texture combinations associated with the glacier surface (Bishop et al., 1995). In an attempt to characterize the structural characteristics of the glacier surface, six surface classes on the glacier were chosen. These classes represented the most unique textures and patterns in the imagery that could be visually differentiated. Structures of the glacier surface that corresponded to these classes included: (1) serac fields, (2) ogives, (3) reticulated ice hills, (4) upper medial moraines, (5) debris-covered high ablation zones, and (6) debris-covered low ablation zones.

Semivariogram analysis of these features should provide insight into the spatial patterns of reflectance. The transect method was used to calculate semivariograms. The following equation was used:

$$\overline{S}^2(h) = \tfrac{1}{2}m \sum_{i=1}^{m} (\mathrm{dn}_i - \mathrm{dn}_{i+h})^2 \qquad (1)$$

$\overline{S}^2$ is an unbiased estimate of the average semivariance $\gamma(h)$ (Curran, 1988), where, 'dn' is relative reflectance from a single pixel, h represents the sampling lag distance, and m is the number of sampled pairs per lag.

The orientation of transects and different samples from the same landscape unit can yield different estimated semivariograms. Consequently, four transects for each feature were systematically collected based upon image analysis and reference data collected in the field. In addition, the orientation of each transect remained constant (parallel) with respect to general ice flow direction. In this way, structural variations because of significant variations in ice velocity were not sampled. Transect lengths were carefully examined to ensure that a large sample size was used for the calculation of the semivariance for each sample lag distance. Each transect was 1.5 km in length. Transects for each feature were systematically selected to represent the entire length of the feature on the glacier. Given the distribution and length of the surface features, our sampling approach provided comprehensive systematic coverage for each feature. Measured semivariograms were interpreted to determine if semivariogram characteristics could be used to differentiate the surface classes on the glacier.

6.3. Fractal analysis

We used the semivariogram method to generate an estimate of the fractal dimension D. The slope (β) of a best-fit line of the log-transformed semi-

variance function is used and relates to the fractal dimension as $\beta = 4 - 2D$ (Mandelbrot, 1982). The fractal dimension estimated from the semivariance function generated from a transect will fall in the range $1.0 \leq D \leq 2.0$, where larger D values represent greater irregularity in spectral variation. A true Brownian fractal would be linear with no changes in β.

Numerous investigators have indicated that technical problems are involved with the computation of the fractal dimension, as changes in β can be present even though the r^2 value (coefficient of determination) is relatively high (Lam, 1990). Some studies have relied upon visual inspection of log–log plots to identify scale-breaks even though this may introduce subjectivity and influence the magnitude of D. In our analysis, we use slope segment information and a linearity index to objectively identify scale-breaks and, therefore, compute D for glacier surfaces.

Unlike a fractional Brownian function, natural surfaces are likely to exhibit a change in fractal dimension over different ranges of scale. Identification of the ranges in which the fractal dimension remains essentially constant is important, yet difficult. In a general case, given an initial set of data points $\{(x_i, y_i) | i = 1, \cdots, n\}$, we first make a transformation to produce the 'log–log' data $\{(x_i^l, y_i^l) | i = 1, \cdots, n\}$ where $x_i^l = \log x_i$ and $y_i^l = \log y_i$. We are interested in finding ranges $[x_{\min}^l, x_{\max}^l]$ in which the log–log data plot is most linear. In this application, x_i represents the lag distance h_i and y_i represents the semivariance $\overline{S}^2(h)$.

Our method of determining such ranges is a variant of the procedure described by Yokoya et al. (1989). Both methods utilize the linearity measure developed by Otsu (1984):

$$L = \frac{\sqrt{4\mu_{11}^2 + (\mu_{20} - \mu_{02})^2}}{(\mu_{20} - \mu_{02})} \qquad (2)$$

where μ_{02} and μ_{20} represent the variances and μ_{11} the covariance of the $\log(x_i) - \log(y_i)$ data. Note that $0 \leq L \leq 1$ with $L = 1$ only if the data are perfectly linear.

Let L_j^k where $k \geq j + 2$ represent the linearity measure computed over the points in the range $[x_j^l, x_k^l]$ [1]. For a given value of $x_{\min}^l$, the method of Yokoya et al. (1989) is designed to find the first point x_k^l such that $L_{\min}^k > L_{\min}^{k-1}$ and $L_{\min}^k > L_{\min}^{k+1}$, i.e., a local maximum of the linearity measure occurs at x_k^l.

In our analysis we found that this method worked well in some cases, but it did not produce the desired result in others. We, therefore, modified the procedure by weakening the local maximum requirement while incorporating restrictions on changes in slope. Let $S_j = (y_{j+1}^l - y_j^l)/(x_{j+1}^l - x_j^l)$, i.e., the slope of the line segment joining points j and $j + 1$. For a given value of $x_{\min}^l$, our modified procedure finds the first point x_k^l such that $L_{\min}^k > L_{\min}^{k+1}$ and $|S_{k+1} - S_k| > (\text{tol})$ where (tol) is a user-specified tolerance value. In testing we set (tol) to the value 0.15. We found that the relaxation of the local maximum requirement while including the slope restriction provided consistently better results. Additionally we found that the tolerance value on the slope acted as a 'degree of generalization' factor; smaller values for (tol) made the procedure more sensitive whereas larger values provided a greater degree of generalization.

All log plots were visually examined to verify the results of an automated analysis of scale-break. The fractal dimensions were estimated based upon this scale-dependent analysis and the fractal dimension evaluated for its ability to characterize the glacier classes.

7. Results

7.1. Interpretation of semivariograms

Examination of semivariograms indicated that several unique patterns exist in relation to the shape and magnitude of semivariance (Figs. 3–8). Caution must be exercised when interpreting semivariograms, because different samples from the same geomorphic unit can yield different estimated variograms. Sev-

[1] The restriction $k \geq j + 2$ is required since $L_j^j = L_j^j + 1 = 1$ for all values of j.

eral important points regarding interpretation include (Curran, 1988; Woodcock et al., 1988a,b):

1. The shape of the variogram is related to the variability in the size of objects.
2. The range is related to the size of objects.
3. The height of the variogram is related to the spectral variability.
4. Semivariogram parameters may change with the direction of the transect.

Therefore, it must be determined if changes in semivariogram characteristics reflect significant changes regarding the glacier surface.

Most of our measured semivariograms exhibited a classic form, although several semivariograms did exhibit a periodic fluctuation in semivariance at larger sample lag distances (multifrequency form). These semivariograms are associated with ogives and reticulated ice hills. For ogives, transects were selected based upon the relative amount of debris-load and the definition and spacing of ogives. The semivariograms exhibiting the well defined multifrequency form represent those locations on the glacier where the debris-load is relatively low and the ogives are well defined (Fig. 3). The differences in spacing of ogives are reflected in the periodicity of the semivariance with scale. For example, the largest distance from ogive to ogive was associated with Transect 4.

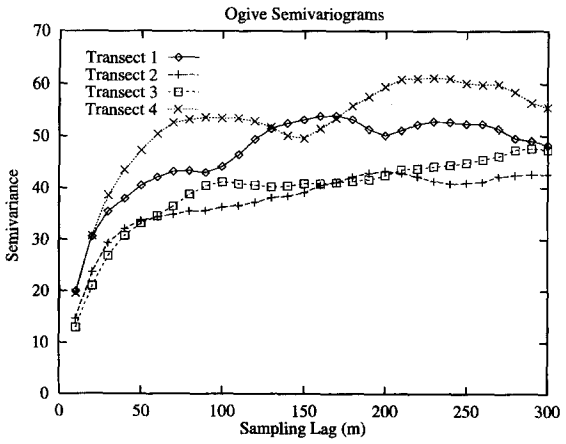

Fig. 3. Semivariograms of ogives. Semivariograms representing Transects 1 and 4 exhibit a multifrequency form. Periodicity of the semivariance is associated with the distance from ogive to ogive. An increase in the presence of debris-load masks the periodicity and results in semivariograms exhibiting a classic form (Transects 2 and 3).

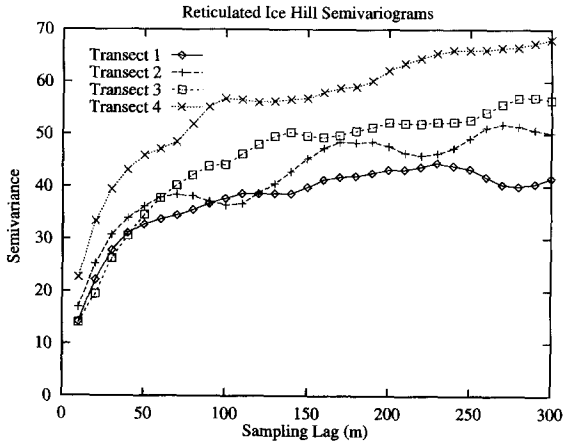

Fig. 4. Semivariograms of reticulated ice hills. Semivariograms from samples along the edge of white-ice streams exhibit relatively high semivariance and a classic form. The semivariogram exhibiting a multifrequency form (Transect 2) represents sampling down the center of the white-ice stream where remnant ogive ice structure may be present. The increased presence of debris-load decreases spectral variability.

Comparison of semivariograms (Transects 1 and 4) indicates that an increase in the frequency of periodicity is associated with closely spaced ogives. In addition, an increase in the presence of debris-load masks the periodicity (e.g., Transects 2 and 3).

It was not anticipated that reticulated ice hill semivariograms would exhibit a multifrequency form (Fig. 4), because the spatial patterns of reflectance appear to be significantly different from patterns associated with ogives (e.g., Transect 2). This particular sample was located a relatively short distance from ogives down the center of the white-ice stream. Other samples were located along the edge of the white-ice stream and further down the glacier. Consequently, periodicity in the semivariogram suggests that the structure down the center of reticulated ice hills at this location is similar to that of ogives, because reticulated ice hills evolve from ogives. Ablation and recrystallization, fracture, and flow of ice cause the reticulated ice patterns. More ablation occurs near the edge of the white-ice stream and further down the glacier, because sediments absorb energy and change the temperature distribution. The ice along the center of the white-ice stream may be minimally affected and, therefore, may retain some of the previous ogive ice structure.

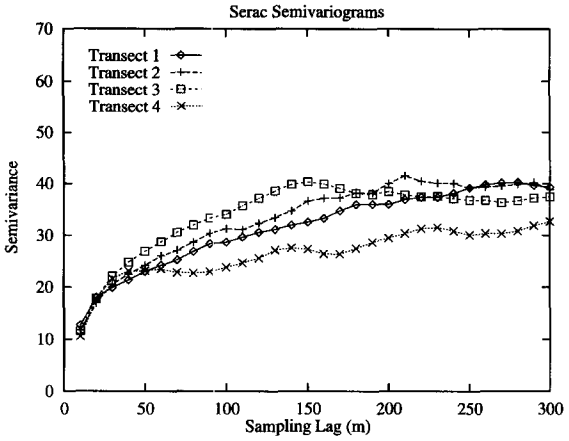

Fig. 5. Semivariograms of serac fields. Spectral variability is relatively high compared to spectral variability of debris-covered features.

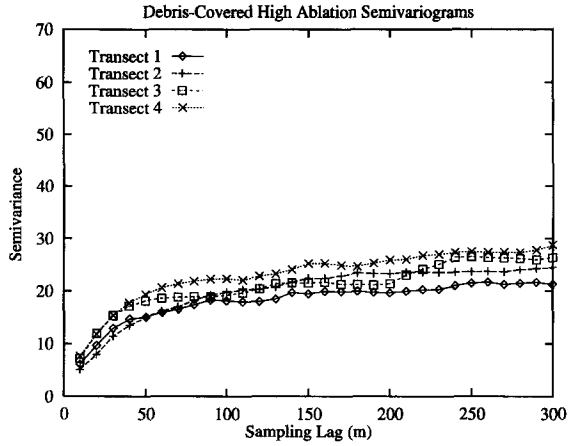

Fig. 7. Semivariograms of debris-covered high ablation zones near the terminus. Spectral variability is relatively low, although the magnitude of the semivariance at various scales is greater than the semivariance associated with debris-covered low ablation zones. This difference in magnitude results from the presence of supraglacial fluvial action which influences spectral variability.

Examination of the height of the variograms indicated that differences in spectral variability exist for some of the classes. As expected, relatively large semivariances were associated with ogives, reticulated ice hills, and seracs (Fig. 5), whereas relatively low semivariances were associated with medial moraines (Fig. 6) and debris-covered surfaces (Figs. 7 and 8). Ogives and reticulated ice hills exhibited the greatest spectral variability, with $\sqrt{S^2}$ values $>$ 30.0 at scales $>$ 50 m. Seracs exhibited $\sqrt{S^2}$ values near 30.0 at scales $>$ 100.0 m, whereas debris-covered classes exhibited the lowest spectral variability with $\sqrt{S^2}$ values $<$ 30.0 across all scales.

Debris-covered classes exhibit similar semivariograms, although spectral variability is higher for high ablation zones versus low ablation zones at various scales. High ablation zones exhibit supraglacial fluvial action and higher ice velocities that increase glacier surface topographic variability. Upper medial moraines do not exhibit as much topo-

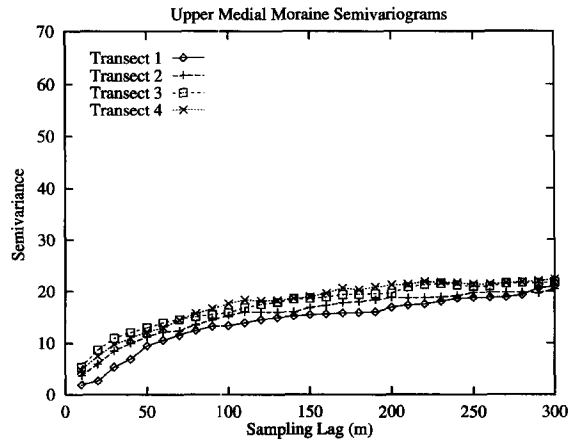

Fig. 6. Semivariograms of upper medial moraines. Spectral variability is very low and semivariograms exhibit a classic form.

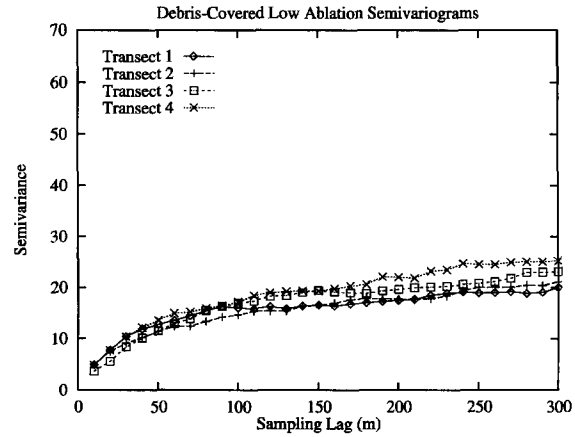

Fig. 8. Semivariograms of debris-covered low ablation zones near the terminus. Spectral variability is relatively low and associated with relatively low ablation and ice velocities.

graphic variability and are lithologically similar. Therefore, these features have the lowest $\sqrt{S^2}$ values at various scales.

7.2. Fractal analysis

Results of fractal analysis indicated that reflectance variation from glacier surfaces did not exhibit fractal behavior (i.e., self-similarity across all scales). With the exception of one transect, the fractal dimension was found to be scale-dependent (i.e., reflectance variation from glacier surfaces exhibited fractal response within scale ranges). Seracs (Transect 1) did exhibit fractal response where spectral reflectance was dominated by white ice and the influence of supraglacial debris cover was minimal ($D = 1.67$). For all other samples, scale-breaks were consistently identified at scales from 30 to 50 m and from 50 to 70 m. These scale-breaks are associated with the scale of lithologic similarity and the spatial frequency of low reflecting ice-cliffs on the surface of the glacier. Consequently, fractal dimensions at scales of 30 and 60 m were tabulated and examined to determine if D values could be used to differentiate glacier surfaces.

Results of fractal analysis (Table 2) show that the magnitude of the fractal dimensions at the 30 m scale (D_{30}) for glacier features are relatively similar. Examination of mean values for each class indicates that reflectance variation from reticulated ice hills and seracs exhibit the greatest 'roughness' or irregularity at this particular scale ($\overline{D}_{30} = 1.44$ and 1.47, respectively). Reflectance variations from ogives were less irregular with a $\overline{D}_{30}$ value of 1.38. Reflectance variations from debris-covered glacier features were very similar with $\overline{D}_{30}$ values near 1.30. These results indicate that because of lithologic similarity at this scale, it would be difficult to differentiate debris-covered features using D_{30} values.

Examination of the fractal dimension at the 60 m scale (D_{60}) indicates that irregularities in reflectance increase with a change in scale. In almost all cases, D_{60} values are larger than D_{30} values. In contrast, relatively large differences in D_{60} values exist for glacier features. For example, a significant difference exists in the average magnitude of $\overline{D}_{60}$ for white-ice-related features versus debris-covered low ablation zones and moraines. These features exhibit highly irregular spectral variation at this scale ($\overline{D}^{O}_{60} = 1.74$; $\overline{D}^{S}_{60} = 1.70$; $\overline{D}^{R}_{60} = 1.68$), whereas moraines and low ablation zone average values are much lower ($\overline{D}^{M}_{60} = 1.47$; $\overline{D}^{L}_{60} = 1.49$). Similarly, debris-covered high ablation zones can be differentiated from debris-covered low ablation zones ($\overline{D}^{H}_{60} = 1.68$). This difference in reflectance variation can be attributed to supraglacial fluvial action that is associated with high ablation near the terminus.

Table 2
Results of fractal analysis

Transect	$D_{\cdot 30}$	r^2_{30}	D_{60}	r^2_{60}
Debris-covered high ablation				
1	1.31	0.99	1.72	0.99
2	1.28	0.99	1.56	0.99
3	1.30	0.99	1.93	0.85
4	1.36	0.99	1.76	0.97
Debris-covered low ablation				
1	1.31	0.99	1.63	0.98
2	1.44	0.99	1.55	0.99
3	1.31	0.99	1.31	0.99
4	1.30	0.99	1.48	0.99
Upper medial moraines				
1	1.07	0.96	1.07	0.96
2	1.30	0.99	1.69	0.92
3	1.35	0.99	1.68	0.99
4	1.36	1.00	1.44	0.98
Ogives				
1	1.46	0.98	1.76	0.99
2	1.36	0.99	1.88	0.99
3	1.33	0.99	1.71	0.98
4	1.37	0.99	1.61	0.99
Reticulated ice hills				
1	1.38	0.99	1.74	0.95
2	1.45	0.99	1.69	0.99
3	1.46	0.99	1.46	0.99
4	1.48	0.99	1.83	0.99
Seracs				
1	1.67	0.99	1.67	0.99
2	1.49	0.99	1.65	0.99
3	1.40	0.99	1.62	0.99
4	1.34	0.99	1.86	0.82

Fractal dimensions of classes of the glacier surface at the 30 and 60 m scales. Results are based upon scale-dependent analysis of log-transformed semivariance functions using slope segment and linearity information.

8. Discussion

Results of semivariogram analysis indicate that the semivariogram can be very useful for assessing global spectral variability for glacier surface classes. White-ice-related features exhibited relatively high semivariance across different scales, and the shape of the semivariograms provided information related to ice structure variations. Similarly, the magnitude of semivariance for debris-covered features provided structural information regarding the spatial variability of low reflecting ice-cliffs. In all cases, the semivariogram was strongly influenced by the spatial variability of debris-load. More research is required to determine if the semivariogram can be used to obtain quantitative information regarding the characteristics of debris-load.

Results also indicate that the fractal dimension has the potential to be useful for studying and classifying supraglacial characteristics. Scale-dependent analysis generates fractal dimensions for scale ranges where unique reflectance patterns may be diagnostic of glacier surface conditions. The appearance of strong breaks in slopes in the variograms of the transect data indicates that reflectance variations for most of the surfaces on the Batura Glacier do not exhibit fractal response, although variations occur in the degree of reflectance irregularity. These results are similar to those found by investigators examining the topographic variation and spectral variation of land-cover units (Mark and Aronson, 1984; Burrough, 1989, 1993; Klinkenberg and Goodchild, 1992). Conversely, the fracturing of white ice, which creates seracs, influences reflectance such that reflectance variation is self-similar across scales.

Developing an automated procedure to make use of spatial features and spatial information is not a simple task. Numerous limitations associated with semivariograms include (De Jong and Burrough, 1995):

1. A large amount of data is required to produce a reliable semivariogram.
2. It is difficult to define the 'criteria of the best model' for estimating semivariogram parameters.
3. Different samples yield different variograms for similar features. This is especially the case when the directionality of the transect is taken into consideration.
4. Using the transect method, no central pixel exists in which semivariogram parameters can be stored.
5. The semivariogram provides global information, but no information on local variation.
6. Current spatial implementation options cause boundary effects and introduce numeric artifacts that are not associated with actual surface feature variation.

Some of these limitations can be viewed as advantageous in attempts to assess glaciers based upon geomorphic criteria. For example, samples in this study were oriented parallel with ice flow direction. A perpendicular orientation would obviously result in a very different semivariogram for that same area, because variations in ice velocity frequently dictate variations in the debris-load. The combination of global information from both orientations would enable unique processes and patterns of the glacier surface to be incorporated into the analysis. Perhaps the most significant limitation associated with this approach is that it does not enable systematic analysis of imagery. Transects have to be spatially confined based upon the size and shape of unique features. Some investigators have utilized the matrix method for calculation of the semivariogram (e.g., Brivo et al., 1993). Other methods also exist for estimating the fractal dimension (Jaggi et al., 1993). Regardless of the method used, systematic spatial analysis of glacier surfaces will require research focusing on spatial implementation options for the calculation of spatial features. More research is required to investigate options for dynamic/adaptive spatial implementation and procedures for multistage pattern recognition that enable the integration of spectral and spatial information for the characterization of the glacier surface.

9. Conclusions

On the basis of geomorphic criteria, SPOT Panchromatic satellite data were used to characterize and differentiate classes of glacier surfaces on a Himalayan glacier. Patterns of spectral reflectance were examined using image semivariance and fractal analysis. Semivariogram analysis, based upon transect data, indicated that the form and magnitude of the semivariogram could describe ice structure and

characteristics of the debris-load. Furthermore, fractal analysis revealed that the fractal dimension has the potential to be used to differentiate some characteristics of the glacier surface. Scale-dependent analysis indicated that reflectance variation from fractured white-ice (seracs) exhibits fractal response, whereas reflectance variations from other glacier surfaces exhibit fractal response only within specific scale ranges. These results indicate that spatial analysis of satellite imagery has the potential to provide detailed information about glacier surfaces in mountainous regions. More research regarding spatial implementation options and the utility of the fractal dimension is underway to make progress towards operational monitoring of Himalayan alpine glaciers, especially around the Nanga Parbat Massif, the focus of our present research.

Acknowledgements

This work was funded by the University Committee on Research at the University of Nebraska at Omaha, National Geographic Society, and the National Science Foundation (Grant No. EAR 9418839). We would like to thank James L. Ward for his assistance in the field.

References

Andrle, R., 1994. The angle measure technique: a new method for characterizing the complexity of geomorphic lines. Math. Geol. 26, 83–97.

Andrle, R., Abrahams, A.D., 1989. Fractal techniques and the surface roughness of talus slopes. Earth Surf. Process. Landf. 14, 197–209.

Batura Glacier Investigation Group (BGIG), 1979. The Batura Glacier in the Karakoram Mountains and its variations. Scien. Sin. 22, 958–974.

Batura Glacier Investigation Group (BGIG), 1980. Karakoram Batura Glacier, Exploration and Research. Lanzhou Inst. of Glaciology and Cryopedology, Academia Sinica, Beijing. Science Press, 271 pp.

Bayr, K.J., Hall, D.K., Kovalick, W.M., 1994. Observations on glaciers in the eastern Austrian Alps using satellite data. Int. J. Remote Sensing 15 (9), 1733–1742.

Bian, L., Walsh, S.J., 1993. Scale dependencies of vegetation and topography in a mountainous environment of Montana. Prof. Geogr. 45 (1), 1–11.

Bishop, M.P., Shroder, J.F. Jr., Ward, J.L., 1995. SPOT multispectral analysis for producing supraglacial debris-load estimates for Batura Glacier, Pakistan. Geocarto Int. 10, 81–90.

Bowers, W.W., Franklin, S.E., Hudak, J., 1994. Forest structural damage analysis using image semivariance. Can. J. Remote Sensing 20, 28–36.

Brest, C.L., Goward, S.G., 1987. Deriving surface albedo measurements from narrow band satellite data. Int. J. Remote Sensing 8, 351–367.

Brivo, P.A., Doria, I., Zilioli, E., 1993. Aspects of spatial autocorrelation of Landsat TM Data for the inventory of waste-disposal sites in rural environments. Photogramm. Eng. Remote Sensing 59 (9), 1377–1382.

Brugman, M.M., Pietroniro, A., Shi, J., 1996. Mapping alpine snow and ice using Landsat TM and SAR imagery at Wapta Icefield. Can. J. Remote Sensing 22, 127–136.

Budd, W.F., Smith, I.N., 1981. The growth and retreat of ice sheets in response to orbital radiation changes. Int. Assoc. Hydrol. Sci. Publ. 131, 369–409.

Burrough, P.A., 1989. Fractals and geochemistry. In: Avnir, D. (Ed.), The Fractal Approach to Heterogeneous Chemistry. Wiley, New York, pp. 383–405.

Burrough, P.A., 1993. Fractals and geostatistical methods in landscape studies. In: Lam, N., De Cola, L. (Eds.), Fractals in Geography. Prentice Hall, Englewood Cliffs, NJ, pp. 87–121.

Chorowicz, J., Kim, J., Manoussis, S., Rudant, J.P., Foin, P., Veillet, I., 1989. A new technique for recognition of geological and geomorphological patterns in digital terrain models. Remote sensing of environment for recognition of geological and geomorphological patterns in digital terrain models. Remote Sensing Environ. 29, 229–239.

Cohen, W., Spics, T., Bradshae, G., 1990. Semivariograms of digital imagery for analysis of conifer canopy structure. Remote Sensing Environ. 34, 167–178.

Conners, R.W., Harlow, C.A., 1980. A theoretical comparison of texture algorithms. IEEE Trans. Pattern Anal. Mach. Intell., PAM 1 (2), 204–222.

Curran, P.J., 1988. The semivariogram in remote sensing. Remote Sensing Environ. 24, 493–507.

Davis, F.W., Quattrochi, D.A., Ridd, M.K., Lam, N.S., Walsh, S.J., Michaelsen, J.C., Franklin, J., Stow, D.A., Johannsen, C.J., Johnston, C.A., 1991. Environmental analysis using integrated GIS and remotely sensed data: some research needs and priorities. Photogramm. Eng. Remote Sensing 57 (6), 689–697.

De Cola, L., 1989. Fractal analysis of a classified Landsat scene. Photogramm. Eng. Remote Sensing 55, 601–610.

De Jong, S.M., Burrough, P.A., 1995. A fractal approach to the classification of Mediterranean vegetation types in remotely sensed images. Photogramm. Eng. Remote Sensing 61, 1041–1053.

Derbyshire, E., Jijun, L., Perrot, F.A., Shuying, X., Waters, R.S., 1984. Quaternary glacial history of the Hunza Valley, Karakoram Mountains, Pakistan. In: Miller, K.J. (Ed.), The International Karakoram Project, 2. Cambridge University Press, Cambridge, pp. 456–495.

Dozier, J., 1984. Snow reflectance from Landsat-4 Thematic Mapper. IEEE Trans. Geosci. Remote Sensing 22, 323–328.

Dozier, J., 1989. Spectral signature of alpine snow cover from the Landsat Thematic Mapper. Remote Sensing Environ. 28, 9–22.

Dozier, J., Marks, D., 1987. Snow mapping and classification from Landsat Thematic Mapper data. Ann. Glaciol. 9, 97–103.

Dutra, L.V., Mascarenhas, N.D.A., 1984. Some experiments with spatial feature extraction methods in multispectral classification. Int. J. Remote Sensing 5 (2), 303–313.

Espizua, L.E., Bengochea, J.D., 1990. Surge of Grande del Nevado Glacier (Mendoza, Argentina) in 1984: its evolution through satellite images. Geogr. Ann. 72 (3/4), 255–259.

Ferrigno, J.G., Lucchitta, B.K., Mullins, K.F., 1993. Velocity measurements and changes in position of Thwaites Glacier/iceberg tongue from aerial photography, Landsat images and NOAA AVHRR data. Ann. Glaciol. 17, 239–244.

Finsterwalder, R., 1937. Die Gletscher der Nanga Parbat. Z. Gletscherkd. Eiszeitforsch. Geschichte Klimas 25, 57–108.

Frank, T.D., 1984. The effect of change in vegetation cover and erosion patterns on albedo and texture of Landsat images in a semiarid environment. Ann. Assoc. Am. Geogr. 74 (3), 393–407.

Fritz, S., 1962. Snow surveys from satellite meteorology. In: Wexler, H. (Ed.), Rocket and Satellite Meteorology. North-Holland, Amsterdam, pp. 419–421.

Gardner, J.S., 1986. Recent fluctuations of Raikhiot Glacier, Nanga Parbat, Punjab Himalaya, Pakistan. J. Glaciol. 32 (112), 527–529.

Gardner, J.S., Jones, N.K., 1993. Sediment transport and yield at the Raikot Glacier, Nanga Parbat, Punjab Himalaya. In: Shroder, J.F., Jr. (Ed.), Himalaya to the Sea. Routledge, London, pp. 184–197.

Goodchild, M.F., 1980. Fractals and the accuracy of geographical measures. Math. Geol. 12, 85–89.

Goodchild, M.F., Mark, D.M., 1987. The fractal nature of geographic phenomena. Ann. Assoc. Am. Geogr. 77, 265–278.

Gratton, D.J., Howarth, P.J., Marceau, D.J., 1990. Combining DEM parameters with Landsat MSS and TM imagery in a GIS for mountain glacier characterization. IEEE Trans. Geosci. Remote Sensing 28, 766–769.

Gratton, D.J., Howarth, P.J., Marceau, D.J., 1993. Using Landsat-5 Thematic Mapper and digital elevation data to determine the net radiation field of a mountain glacier. Remote Sensing Environ. 43 (3), 315–332.

Gregotski, M.E., Jensen, O., 1993. Fractal modeling techniques for spatial data. IEEE Trans. Geosci. Remote Sensing 31, 980–988.

Hall, D.K., Bindschadler, R.A., Ormsby, J.P., Siddalingaiah, H., 1987. Characterization of snow and ice reflectance zones on glaciers using Landsat Thematic Mapper data. Ann. Glaciol. 9, 104–108.

Hall, D.K., Chang, A.T.C., Siddalingaiah, H., 1988. Reflectances of glaciers as calculated using Landsat Thematic Mapper data. Remote Sensing Environ. 25, 311–321.

Hall, D.K., Chang, A.T.C., Foster, J.L., Benson, C.S., Kovalick, W.M., 1989. Comparison of in situ and Landsat derived reflectance of Alaskan glaciers. Remote Sensing Environ. 28, 23–31.

Hall, D.K., Bindschadler, R.A., Foester, J.L., Chang, A.T.C., Siddalingaiah, H., 1990. Comparison of in situ and satellite-derived reflectances of Forbindels Glacier. Greenland. Int. J. Remote Sensing 11 (3), 493–504.

Haralick, R.M., 1979. Statistical and structural approaches to texture. Proc. IEEE 67, 768–804.

Haralick, R.M., Shanmugam, K., Dinstein, I., 1973. Textural features for image classification. IEEE Trans. Syst., Man, Cybernetics, SMC 3, 610–621.

Harbor, J.M., 1992. Application of a general sliding law to simulating flow in a glacier cross section. J. Glaciol. 38 (128), 182–190.

Harris, R., 1980. Spectral and spatial image processing for remote sensing. Int. J. Remote Sensing 1 (4), 361–375.

Hastenrath, S., 1993. Toward the satellite monitoring of glacier changes on Mount Kenya. Ann. Glaciol. 17, 245–249.

Herzfeld, U.C., Lingle, C.S., Lee, L., 1993. Geostatistical evaluation of satellite radar altimetry for high-resolution mapping of Lambert Glacier, Antarctica. Ann. Glaciol. 17, 77–85.

Irons, J.R., Petersen, G.W., 1981. Texture transforms of remotely sensed data. Remote Sensing Environ. 11, 359–370.

Jaggi, S., Quattrochi, D.A., Lam, N.S., 1993. Implementation and operation of three fractal measurement algorithms for analysis of remote sensing data. Comput. Geosci. 19, 745–767.

Klinkenberg, B., Goodchild, M.F., 1992. The fractal properties of topography: a comparison of methods. Earth Surf. Process. Landf. 17, 217–234.

Koelemeijer, R., Oerlemans, J., Tjemkes, S., 1993. Surface reflectance of Hintereisferner, Austria, from Landsat 5 TM imagery. Ann. Glaciol. 17, 17–22.

Krimmel, R.M., Meier, M.F., 1973. Glacier applications of ERTS images. J. Glaciol. 15 (73), 391–402.

Kulkarni, A.V., 1992. Mass balance of Himalayan glaciers using AAR and ELA methods. J. Glaciol. 38, 101–104.

Lam, N.S., 1990. Description and measurement of Landsat TM images using fractals. Photogramm. Eng. Remote Sensing 56, 187–195.

Lam, N.S., Quattrochi, D.A., 1992. On the issues of scale, resolution, and fractal analysis in the mapping sciences. Prof. Geogr. 44, 88–98.

Laws, K.I., 1980. Texture image segmentation. Dep. of Electrical Engineering, Image Processing Inst., Univ. of California at Los Angeles, Los Angeles, CA, USCIPI Rep. 194.

Lefauconnier, B., Hagen, J.O., Rudant, J.P., 1994. Flow speed and calving rate of Kongsbreen Glacier, Svalbard, using SPOT images. Polar Res. 13 (1), 59–65.

Lucchitta, B.K., Mullins, K.F., Allison, A.L., 1993. Antarctic glacier-tongue velocities from Landsat images: first results. Ann. Glaciol. 17, 356–366.

Mandelbrot, B.B., 1982. The Fractal Geometry of Nature. Freeman, New York.

Mark, D.M., Aronson, P.B., 1984. Scale-dependent fractal dimensions of topographic surfaces: an empirical investigation, with applications in geomorphology and computer mapping. Math. Geol. 16 (7), 671–683.

McDermid, G.J., Franklin, S.E., 1995. Remote sensing and geomorphometric discrimination of slope processes. Z. Geomorphol. N.F. 101, 165–185.

Mulla, D.M., 1988. Using geostatistics and spectral analysis to study spatial patterns in the topography of southwestern Washington State. Earth Surf. Process. Landf. 13, 389–405.

Nakawo, M., Morohoshi, T., Uehara, S., 1993. Satellite data utilization for estimating ablation of debris covered glaciers. Int. Assoc. Hydrol. Sci. Publ. 218, 75–83.

Olsen, E.R., Ramsey, R., Winn, D.S., 1993. A modified fractal dimension as a measure of landscape diversity. Photogramm. Eng. Remote Sensing 59, 1517–1520.

Ostrem, G., 1975. ERTS data in glaciology—an effort to monitor glacial mass balance from satellite imagery. J. Glaciol. 15, 403–415.

Otsu, N., 1984. Karhunen–Loeve line fitting and a linearity measure. Proc. 7th Int. Conf. Pattern Recognition, pp. 486–489.

Parrot, J.F., Lyberis, N., Lefauconnier, B., 1993. SPOT multispectral data and digital terrain model for the analysis of ice–snow fields on Arctic glaciers. Int. J. Remote Sensing 14 (3), 425–440.

Polidori, L., Chorowicz, J., Guillande, R., 1991. Description of terrain as a fractal surface, and application to digital elevation model quality assessment. Photogramm. Eng. Remote Sensing 57, 1329–1332.

Roach, D., Fung, K.B., 1994. Fractal-based textural descriptors for remotely sensed forestry data. Can. J. Remote Sensing 20, 59–70.

Rosenfeld, A., 1980. Terrain classification using texture analysis. Proc. Soc. Photo-Opt. Instrum. Eng. 238, 358–360.

Ryherd, S., Woodcock, C., 1996. Combining spectral and texture data in the segmentation of remotely sensed data. Photogramm. Eng. Remote Sensing 62 (2), 181–195.

Sali, E., Wolfson, H., 1992. Texture classification in aerial photographs and satellite data. Int. J. Remote Sensing 13 (18), 3395–3408.

Scambos, T.A., Dutkiewicz, M.J., Wilson, J.C., 1992. Application of image cross correlation to the measurement of glacier velocity using satellite image data. Remote Sensing Environ. 42 (3), 177–186.

Shih, E.H., Schowengerdt, R.A., 1983. Classification of arid geomorphic surfaces using Landsat spectral and textural features. Photogramm. Eng. Remote Sensing 49 (3), 337–347.

Shroder, J.F. Jr., 1989. Hazards of the Himalaya. Am. Sci. 77, 564–573.

Shroder, J.F. Jr., Owen, L., Derbyshire, E., 1993. Quaternary glaciation of the Karakoram and Nanga Parbat Himalaya. In: Shroder, J.F., Jr. (Ed.), Himalaya to the Sea. Routledge, London, pp. 132–158.

Sigurdsson, O., 1994. Comments on 'Analysis of glacier facies using satellite techniques' by Williams et al. J. Glaciol. 40, 202–203.

Singer, S.F., Popham, R.W., 1963. Non-meteorological observations from weather satellites. Astronaut. Aerospace Eng. 1 (3), 89–92.

Singhroy, V.H., Kenny, F.M., Barnett, P.J., 1992. Radar imagery for Quaternary geological mapping in glaciated terrains. Can. J. Remote Sensing 18 (2), 112–117.

Tarble, R.D., 1963. Areal distribution of snow as determined from satellite photographs. Int. Assoc. Sci. Hydrol. Publ. 65, 373–375.

Ventura, A.D., Rampini, A., Rabagliati, R., Barbero, R.S., 1987. Development of a satellite remote sensing technique for the study of alpine glaciers. Int. J. Remote Sensing 8 (2), 203–215.

Vohra, C.P., Aggarwal, N.K., 1981. Glacier inventory from satellite imagery in a Himalayan situation. Z. Gletscherkd. Glazialgeol. 17, 199–204.

Wang, L., He, D.C., 1990. A new statistical approach for texture analysis. Photogramm. Eng. Remote Sensing 56, 61–66.

Wang, S., Elliott, D.B., Campbell, J.B., Erich, R.W., Haralick, R.M., 1983. Spatial reasoning in remotely sensed data. IEEE Trans. Geosci. Remote Sensing GE 21 (1), 94–101.

Weszka, J.S., Dyer, C.R., Rosenfeld, A., 1976. A comparative study of texture measures for terrain classification. IEEE Trans. Syst., Man, Cybernetics, SMC 6 (4), 269–285.

Williams, R.S. Jr., Hall, D.K., Benson, C.S., 1991. Analysis of glacier facies using satellite techniques. J. Glaciol. 37 (125), 120–128.

Woodcock, C.E., Strahler, A.H., Jupp, D.L.B., 1988a. The use of variograms in remote sensing, I. Scene models and simulated images. Remote Sensing Environ. 25, 323–348.

Woodcock, C.E., Strahler, A.H., Jupp, D., 1988b. The use of variograms in remote sensing. Remote Sensing Environ. 25, 323–379.

Yokoya, N., Yamamoto, K., Funakubo, N., 1989. Fractal-based analysis and interpolation of 3D natural surface shapes and their application to terrain modeling. Comput. Vision, Graphics, Image Process. 46, 284–302.

Zeitler, P.K., 1985. Cooling history of the NW Himalaya, Pakistan. Tectonics 4, 127–151.

Zeitler, P.K., Chamberlin, C.P., 1991. Petrogenetic and tectonic significance of young leucogranites from the northwestern Himalaya, Pakistan. Nature 298, 255–257.

Zhang, X., Shi, Y., 1980. Changes of the Batura Glacier in the Quaternary and recent times. In: Karakoram Batura Glacier, Exploration and Research. Lanzhou Inst. of Glaciology and Cryopedology, Academica Sinica, Beijing. Science Press, pp. 173–190.